AGU ADVANCING EARTH AND SPACE SCIENCE

Geophysical Research Letters

Key Points:

- No significant change in the overall temperature sensitivity of high northern latitude spring greenness in the past 40 years
- Decreased spatial coherence of spring temperature anomalies has increased the influence of atmospheric transport on surface CO_2 data
- Temperature sensitivity of spring carbon uptake remains strong when accounting for atmospheric transport

Supporting Information:

- Supporting Information S1

Correspondence to:

P. Joyce,
eepjj@leeds.ac.uk

How Robust Is the Apparent Break-Down of Northern High-Latitude Temperature Control on Spring Carbon Uptake?

Peter Joyce[1] , Roel Brienen[1] , Wolfgang Buermann[2], Chris Wilson[3,4] , Martyn P. Chipperfield[3,4] , Mariona Claret[5] , and Manuel Gloor[1]

[1]School of Geography, University of Leeds, Leeds, UK, [2]University of Augsburg, Augsburg, Germany, [3]School of Earth and Environment, University of Leeds, Leeds, UK, [4]National Centre for Earth Observation, University of Leeds, Leeds, UK, [5]Cooperative Institute for Climate, Ocean, and Ecosystem Studies, University of Washington, Seattle, WA, USA

Abstract Vegetation growth in northern high-latitudes during springtime is strongly temperature limited, and thus anomalously warm springs are expected to result in an increased drawdown of carbon dioxide (CO_2). However, a recent analysis of the relationship between spring temperature anomalies and atmospheric CO_2 anomalies at Point Barrow, Alaska, suggests that the link between spring carbon uptake by northern ecosystems and temperature anomalies has been weakening over recent decades due to a diminishing control of temperature on plant productivity. Upon further analysis, covering the 1982–2015 period, we found no significant change in the relationship between spring vegetation productivity derived from remote sensing data and air temperature. We showed that a reduction in spatial coherence of temperature anomalies, alongside a significant sensitivity to atmospheric transport, is likely responsible for the apparent weakening. Our results, therefore, suggest that spring temperature remains as an important control of northern high-latitude CO_2 uptake.

Plain Language Summary The timing of the vegetation growing season is strongly linked to the quantity of carbon dioxide (CO_2) absorbed each year, however, it is unclear how this will evolve. The spring zero crossing (SZC) of atmospheric CO_2 is an indicator of how early the growing season starts. This is because the growing season is characterized by a significant photosynthetic drawdown of CO_2 by vegetation. This quantity has historically been strongly controlled by temperature in northern high-latitude ecosystems. A recent study analyzed surface CO_2 data at a site in Alaska and suggested that this control has broken down. We show here, using satellite-based vegetation data, that there has been no change in the control of temperature on vegetation productivity across the high northern latitudes. We then demonstrate that the temperature anomalies became more spatially variable across the northern high latitudes in recent decades and that variations in atmospheric circulation lead to different regions of influence over the Alaskan CO_2 site. These influences play a key role in the year-to-year variability of the SZC and its relationship with temperature. Our study demonstrates that the control of temperature on the year-to-year variations in the timing and magnitude of spring CO_2 uptake has remained strong.

1. Introduction

Land vegetation has been a significant sink of atmospheric CO_2 over past decades, taking up roughly a quarter of emissions from fossil fuels and land-use change (Friedlingstein et al., 2019). Toward the end of the 20th century, the Arctic and boreal ecosystems took up between 0.3 and 0.6 PgC yr^{-1} – representing a significant fraction of the global land sink of 1.0 PgC yr^{-1} during this period based on top-down and bottom-up carbon budget estimates (McGuire et al., 2009). Previous studies also indicate that this northern carbon sink has also accelerated in recent decades (Ciais et al., 2019; Wang et al., 2013). In a warming world, it is important to understand how the relationship between climate and carbon uptake in the northern high-latitudes is evolving if we are to understand the future behavior of the land carbon sink.

A valuable metric for understanding the carbon cycle in the northern hemisphere is the atmospheric CO_2 seasonal cycle. This cycle exhibits a yearly maximum during the colder months when CO_2 release processes (respiration) dominate, and a yearly minimum during the warmer months when photosynthesis dominates. Keeling et al. (1996) noted that the amplitude of CO_2 seasonal cycle (defined as the difference between

annual maximum and minimum) has been increasing over time and that the fastest changes were occurring in northern high latitudes. They also showed that the increase in the CO_2 seasonal amplitude was correlated with northern temperature anomalies and accompanied by a phase advance during the declining phase of the seasonal cycle of CO_2 giving rise to the hypothesis that longer growing seasons are associated with warmer temperatures. A more recent analysis of global CO_2 records confirms that this phenomenon is continuing, showing that the CO_2 seasonal amplitude at the Barrow (Nuvuk) Observatory in Alaska (hereafter referred to as Barrow) increased by 0.60% per year from 1961 to 2011 (Graven et al., 2013).

Respiration and photosynthesis are both strongly affected by temperature, and the competition between them is expected to lead to different responses of net carbon uptake to temperature throughout the year. Observational and model evidence suggest that warming during spring leads to increased carbon uptake while warming during autumn leads to decreased carbon uptake during each respective period (Piao et al., 2008; Randerson et al., 1999). This is explained by the stronger response of photosynthesis (relative to respiratory processes) to warming during springtime, whereas in fall the respiration sensitivity to warming exceeds that of photosynthesis (Piao et al., 2008).

Recently, Piao et al. (2017) (hereafter P2017) showed that the springtime relationship between northern high-latitude temperature and concurrent CO_2 uptake (inferred from atmospheric CO_2 data measured at Barrow) has substantially weakened since the mid-1990s. In their study, this phenomenon was attributed to a weakening of the temperature control on plant productivity based on factorial simulations with biospheric and atmospheric transport models (P2017). These results, therefore, challenge the *"warmer spring – larger carbon sink mechanism,"* and may be indicative of approaching a new regime in which other climatic constraints, such as *"reduced chilling during dormancy,"* and *"an emerging light limitation,"* play a more dominant role in determining spring carbon uptake across northern land (P2017).

While these results are intriguing, influences of atmospheric circulation pattern on findings that are based on single CO_2 monitoring stations cannot be ruled out. The Arctic Oscillation (AO), an atmospheric circulation regime which has a powerful influence over wind patterns and near-surface climate patterns in the high northern latitudes (Thompson & Wallace, 1998), could play an important role here. In this regard, it is notable that the change in correlation between spring vegetation activity and temperature between the two focal periods 1982–1996 and 1997–2012 (which we refer to as the early/late period), as shown in Figure 3j of P2017, has a spatial pattern that strongly resembles an AO pattern (Figure S1). This led us to investigate further if the apparent weakening temperature control on spring carbon uptake (P2017) was influenced by large-scale atmospheric circulation patterns.

P2017 investigated the effect of holding land fluxes constant while atmospheric transport varies. They analyzed the spring zero crossing (SZC), an indicator of the timing and magnitude of spring carbon uptake by land vegetation. P2017 found that the correlation between the SZC and temperature reduces significantly during the early period (when compared with the control), although there is still a clear difference in correlation between the two time periods. However, there is no simulation in P2017 in which transport is held constant, so it is not possible to determine the strength of the interaction effect between land fluxes and transport.

We therefore aim to explore the role of atmospheric transport in the apparent weakening of the link between spring time northern temperatures and carbon uptake in more detail. Unlike P2017, we used interannually varying footprints of Barrow during spring calculated with the HYSPLIT4 atmospheric trajectory model (Stein et al., 2015) to better understand corresponding influences. To gain additional information on the drivers of spring carbon uptake across northern land, we then performed factorial forward simulations combining modeled land-atmosphere carbon flux exchanges (based on the Carnegie-Ames-Stanford Approach (CASA) land-surface model (Potter et al., 1993; Randerson et al., 1996)) and the TOMCAT atmospheric chemistry-transport model (Chipperfield, 2006).

2. Materials and Methods

2.1. Atmospheric CO_2 and Analysis of SZC

We analyzed the daily in-situ CO_2 record at the Barrow Observatory, Alaska (71°N, 156°W) from the National Oceanic and Atmospheric Administration (NOAA) Earth Research Laboratory/Global Monitoring Division program (Thoning et al., 2020). The raw CO_2 data were smoothed using the Carbon Cycle Group CuRVe (CCGCRV) routine (Thoning et al., 1989), from which we obtained the detrended smoothed seasonal cycle (see Text S2). The SZC is defined as the day of the year when the CO_2 levels pass through zero in the detrended smoothed seasonal cycle. Similarly, an additional metric for spring carbon uptake known as spring carbon capture (SCC) is calculated from the difference between the first week of May and last week of June in the detrended smoothed seasonal cycle. Our definition of early and late period shifts to 1979–1995 and 1996–2012, respectively, when analyzing SZC and SCC due to the availability of data during the 1979–1981 period.

2.2. Climate and Vegetation Data

Satellite NDVI (or greenness) data were used as a proxy for vegetation productivity. Monthly data were obtained from the Global Inventory Modeling and Mapping Studies (GIMMS) Version 3g Advanced Very-High Resolution Radar (AVHRR) data set (Pinzon & Tucker, 2014) over the 1982–2015 period, means-aggregated to a spatial resolution of 0.25° (from their native resolution of 8 km). An additional satellite product used as a proxy for productivity is the Fraction of Photosynthetically Active Radiation (FPAR) (Zhu et al. (2013). Monthly 0.5° resolution air temperature, precipitation and cloud cover data were taken from the Climatic Research Unit TS 4.01 data sets (https://crudata.uea.ac.uk/cru/data/hrg/; Harris et al., 2014), during the 1979–2016 period, with spatial averages calculated over vegetated land, indicated by an NDVI value greater than 0.1. During years in which no NDVI data were available (1979–1981 and 2016), the NDVI > 0.1 mask was calculated from averages taken of the 3 chronologically closest years. For calculating the detrended spatial average of NDVI and climate data, we detrended the data at each pixel, then summed over the region of interest. The AO data set was obtained from December to March averages taken from the NOAA teleconnections data set. More information is available from https://www.cpc.ncep.noaa.gov/products/precip/CWlink/daily_ao_index/ao.shtml.

2.3. HYSPLIT4 Footprints

Back trajectories, calculated using National Centers for Environmental Prediction meteorological data, were used to track the source of the springtime CO_2 signal. Trajectories starting at Barrow during the March–June period were computed every 6 h. Each back trajectory was extended 30 days backwards in time with locations sampled every hour. For footprint-weighting of temperature and NDVI, we multiplied the temperature and NDVI respectively by the monthly average footprint (units of hours), before averaging the March–June value for each year.

2.4. Factorial Simulations

We used an observation-based modeling approach to simulate atmospheric CO_2 at Barrow with the CASA land-surface model feeding Net Ecosystem Exchange (NEE) fluxes into the TOMCAT atmospheric chemistry model.

CASA uses a simple light-use efficiency approach to estimate Net Primary Productivity (NPP) as follows:

$$NPP = FPAR * SOLRAD * LUEmax * temp\_scalar * moisture\_scalar * SC \qquad (1)$$

where *FPAR* is the fraction of photosynthetically active radiation, *SOLRAD* is ECMWF ERA-Interim 1D solar radiation (Dee et al., 2011), *LUEmax* is the maximum light use efficiency which is based on estimated values for each biome type, the temperature and moisture scalars reduce NPP proportional to their deviation from optimal values, and solar conversion (SC) converts to solar units. NPP of herbaceous and woody vegetation is calculated separately with different moisture scalars. CASA uses a series of first-order, linear

differential equations to calculate heterotrophic respiration and the flow of carbon between each of the soil and vegetation pools.

The NEE fluxes from CASA were applied as surface boundary conditions in TOMCAT, as well as fossil fuel emissions from the Carbon Dioxide Information Analysis Center (Andres et al., 2016) and monthly air-sea CO_2 gas fluxes from an ice-ocean-biogeochemical coupled model of the NOAA Geophysical Fluid Dynamics Laboratory forced with COREv2 normal year atmospheric forcing and historical CO_2 atmospheric concentrations (Claret et al., 2021). TOMCAT used ECMWF ERA-Interim meteorology (Dee et al., 2011), running on a 2.8° horizontal grid with 60 vertical levels up to 0.1 hPa to simulate transport and mixing of atmospheric CO_2. Simulated CO_2 concentrations were then sampled at the locations of the measurement sites every 6 h, after which, daily averages were taken, and the simulated daily CO_2 time series treated identically to the observed CO_2 data outlined in Section 2.1.

We conducted several experiments where we changed components of the CASA model. Specifically, we performed simulations in which we kept the following CASA driver variables at their climatological mean values (with their referenced names in parentheses): Temperature scalar (*TMP*), temperature and moisture scalars (*TMO*), solar radiation (*SLR*), the fraction of absorbed photosynthetically active radiation (a satellite product indicative of assimilation of CO_2 by vegetation - see Section 2.2) (*FPAR*), all of those previously mentioned (*ALL*). We then repeated these experiments with atmospheric transport repeating itself every year (using 2006 meteorology). The runs using annually repeating transport fields are referred to with the "*AT,*" prefix. For example, *AT,TMP* is the run with annually repeating transport and temperature. It should be noted that the temperature variable in CASA only influences NPP through temperature stress (the *temp_scalar* term from Equation 1), with the positive effects of temperature on productivity being modulated through FPAR. Similarly, the moisture scalars only relate to moisture stress in NPP.

3. Results and Discussion

3.1. Temperature Sensitivity of SZC and NDVI

In a first step, we reproduced and extended the analysis of P2017 by 4 years up to 2016 and compared the timing of the detrended CO_2 spring zero crossing (SZC) of the seasonal cycle of atmospheric CO_2 at Barrow with the spatially averaged (all vegetated land north of 50°N) detrended spring temperature. Our results are consistent with those from P2017 and show for the 1979–1995 time period the strong correlation between detrended SZC at Barrow and spring March–June temperature (Figure 1a). However, and as pointed out by P2017, after 1996 this relationship weakens substantially (Figures 1a and 1b). P2017 repeated their analyses with SCC and obtained the same result. We also repeated this analysis with SCC (Text S1), confirming their conclusion.

We next analyzed a similar relationship between springtime temperature and NDVI, a satellite-based proxy of photosynthetic activity (Pinzon & Tucker, 2014). In contrast to the SZC-temperature relationship, we found that the correlation between the 50°N spatial average of springtime NDVI and temperature does not weaken significantly over time (Figures 1c and 1d). The relationship between spring vegetation productivity and satellite-based NDVI (or greenness) is not straightforward with actual onset of photosynthesis potentially lagging spring green up (estimated from NDVI) depending on land cover type (Walther et al., 2016). However, these results do not support the hypothesized weakening of the temperature control of high latitude plant productivity during springtime put forward by P2017, opening the door for alternative explanations for the breakdown of the SZC-temperature relationship.

One possible explanation is that interannually varying atmospheric transport contributes to the decoupling of detrended SZC and spring temperature. This is because the CO_2 signal recorded at Barrow has a spatial footprint representative of a limited region of influence, whereas the relationship between detrended NDVI anomalies and detrended temperature anomalies is based on the entire region above 50°N. In the P2017 analysis, the temperature record used is a zonal average across vegetated lands north of 50°N, which assumes that the atmospheric footprint of Barrow is influenced uniformly and exclusively by land in this zonal band for all years in the study period. This is despite their footprint analysis of Barrow demonstrating significantly larger contributions from fluxes in Alaska and Eastern Eurasia to the Barrow record than other high-northern latitude regions (P2017).
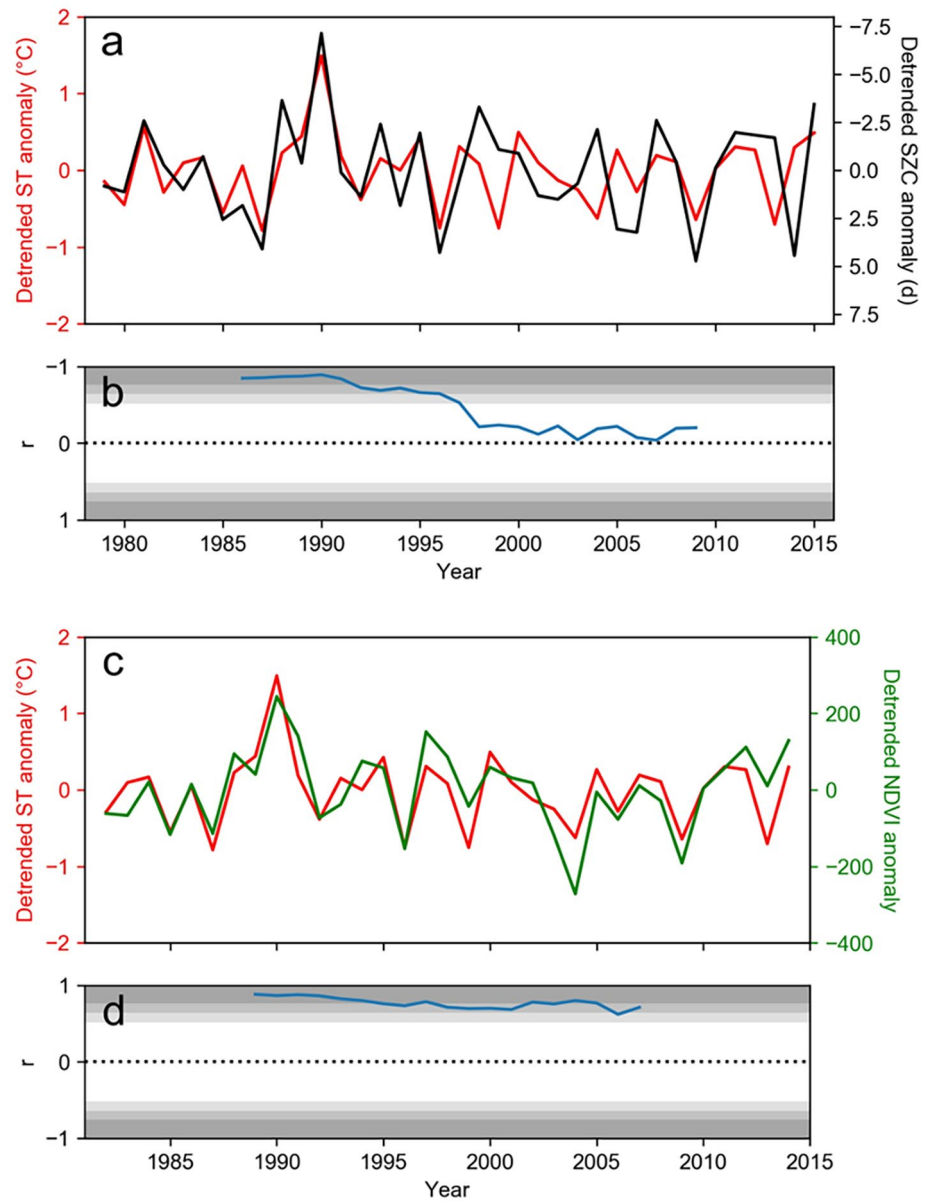
Figure 1. Time series of the anomaly (°C) in detrended spring (March to June) temperature (ST) averaged across vegetated land north of 50°N along with (a) detrended SZC (days) at Barrow and (c) detrended spring NDVI (March to June) averaged over vegetated land north of 50°N. Panels (b) and (d) show corresponding moving window (15 years) partial correlations (accounting for precipitation and radiation). Shaded regions depict 5%, 1%, and 0.1% significance levels ($n = 15$).

3.2. Footprint of Barrow

In a next step, we analyzed the influence of variations in atmospheric transport on CO_2 concentrations at Barrow using the HYSPLIT4 trajectory model (hereafter referred to as "Hysplit"). Hysplit footprints revealed strong spatial variation in the origin of the air arriving at Barrow (Figure S2). We found disproportionately large contributions from Alaska and up to 10% of the signal coming from vegetated land south of 50°N. This suggests potential pitfalls with relating CO_2 data at Barrow to temperature data averaged uniformly over land north of 50°N.

We also observed significant interannual variability in the regions influencing Barrow (Figure S3), with contributions from Eurasia ranging from 30% to 65% of the total land footprint. These results suggest that

atmospheric transport may have a strong influence on the variability of CO_2 sampled at Barrow. These findings are also in line with previous studies highlighting the necessity to account for changing circulation patterns when inferring carbon dynamics from single-site analyses (Buermann et al., 2007; Wang et al., 2020).

Nonetheless, when we weighted the temperature, precipitation, and cloud cover (a proxy for solar radiation) data using interannually varying Barrow footprints (see Section 2.3), we found that the strong decoupling of the springtime temperature-SZC relationship after 1995 is retained (Figure S4a). Furthermore, we found that the springtime temperature sensitivity of vegetation productivity has weakened slightly more inside the footprint of Barrow than across the high latitudes as a whole (Figure S4c and Figure 1b) although this weakened relationship inside the Barrow footprint occurs only from 2003 onwards and is also statistically not very robust (Figure S4b).

3.3. Spatial Variability of Temperature

An ensuing analysis of the influence of atmospheric transport on the temperature-SZC relationship showed that the method for averaging temperature (Barrow footprint-weighted vs. all vegetated land above 50°N) is unimportant in the early period 1979–1995 (corresponding temperature time series correlate strongly), but during the later period, these temperature time series diverge (Figure S5). This result points toward greater spatial variability in the temperature signal and thus an increase in the importance of atmospheric transport in the later period.

To understand the reason for this behavior, we looked at the spatial distribution of spring temperature anomalies. To do so, we compared the anomalies in the detrended large-scale mean spatial average temperature (across all vegetated regions above 50°N) with the detrended spring temperatures at each pixel. Temperature anomalies for the period 1979–1995 generally agreed well with the spatial mean (mean correlation averaged over all pixels, $\overline{r} = 0.37$), but there was a shift in the second period toward less coherent temperature correlation pattern ($\overline{r} = 0.27$) (Figure S5). If the correlations are weighted by the time-varying Barrow footprint, the correlation is even stronger in the early period ($\overline{r} = 0.42$) and breaks down more significantly in the later period ($\overline{r} = 0.21$).

These results suggest that during the later period, the high latitude temperature anomalies are less coherent across large spatial scales and the footprint as seen by Barrow is less representative of the entirety of the high northern latitudes (Figures S6 and S5). The strong coherence in large-scale temperature anomalies in the early period (before the mid-1990s) may be due to the strong activity of the AO. During 1979–1995, the AO index maintained prolonged periods in its negative and positive phase, which promoted large-scale temperature coherence especially in footprint regions of Barrow (Figures S1 and S2). In contrast, during the later period, such extended periods of persistent AO phases were absent. Another indication for a strong AO influence during the early period is that the spatial pattern of correlations between local and large-scale springtime temperature signals in the early period (Figure S5) is to a large extent reminiscent of the correlation pattern between spring temperature and the AO index (Figure S1b).

The strong spatial coherence of temperature in the early period minimizes the influence of transport on CO_2 sampled at Barrow. In contrast, during the later period, transport will have been more important provided the CO_2 signal (as a result of land NEE) was more spatially variable as indicated by greater spatial variability in spring temperature (Figure S5).

The springtime temperature sensitivity of vegetation green-up exhibits significant nonlinear behavior across the high latitudes (Park et al., 2015). Across the same region, there is also significant variability in the temperature sensitivity of spring productivity, as indicated by a regression between spring NDVI and temperature (Figure S7). The sensitivity of NDVI to temperature during springtime is more spatially variable in the later period (standard deviation of the sensitivity, $\sigma = 95.5°C^{-1}$) than the early period ($\sigma = 78.1°C^{-1}$) (Figure S6), hence exacerbating the effects of the reduced spatial coherence in temperature (Figure S5). As a result, in the later period when temperature coherence is reduced, the correlation between temperature averaged over Barrow footprints and SZC at Barrow would decrease, independently from a decrease in temperature sensitivity of vegetation productivity.

Table 1
Correlations Between Simulated SZC From Factorial Simulations With Observed SZC and Spring Temperature

Simulation	Correlation of simulated SZC with complete model, and model with variables held constant		Partial correlation of simulated SZC with footprint-averaged observed spring temperature		Partial correlation of simulated SZC with 50°N-averaged observed spring temperature	
	1982–1996	1997–2012	1982–1996	1997–2012	1982–1996	1997–2012
Control Run (CTRL)	N/A	N/A	−0.83***	−0.47	−0.85***	−0.16
Variable(s) held constant						
Temperature scalar (TMP)	0.95***	0.92***	−0.74**	−0.53*	−0.69**	−0.05
Temperature and Moisture scalars (TMO)	0.95***	0.92***	−0.75*	−0.51*	−0.70**	−0.12
Solar Radiation (SLR)	0.89***	0.95***	−0.87***	−0.32	−0.82***	−0.12
FPAR	0.82***	0.67**	−0.54*	−0.05	−0.54*	−0.08
TMO, SLR and FPAR (ALL)	0.82***	0.70**	−0.74**	−0.07	−0.63*	0.00
Transport (AT,CTRL)	0.74**	0.43	−0.55*	−0.50	−0.50	−0.18
Transport and Temperature scalar (AT,TMP)	0.75**	0.33	−0.55*	−0.61*	−0.54*	−0.27
Transport and Temperature and Moisture scalars (AT,TMO)	0.75**	0.44	−0.58*	−0.62*	−0.49	−0.29
Transport and Solar Radiation (AT,SLR)	0.67**	0.39	−0.73**	−0.25	−0.73**	−0.02
Transport and FPAR (AT,FPAR)	0.06	−0.07	0.03	−0.05	0.18	0.00
Transport, TMO, SLR and FPAR (AT,ALL)	0.22	−0.15	−0.24	0.07	−0.01	0.24

The notations *, ** and *** indicate significance at 5%, 1%, and 0.1% levels, respectively. Values over the 1997–2012 period are taken from the median correlation value after systematically removing each year from the chronology. Partial correlations take precipitation and cloud cover into account. The constant transport runs are referred to with the "AT" prefix. Detailed plots on each of the simulations in supplementary materials (Figures S10–S20).

3.4. Factorial Simulations

To further examine the relative influence of vegetation productivity (NPP) and atmospheric transport on the link between detrended SZC and spring temperatures, we conducted factorial forward simulations with land-based carbon NEE fluxes (based on the CASA model) feeding into the TOMCAT atmospheric chemistry-transport model (see Methods). Results based on a control run (hereafter referred to as CTR) in which all model drivers (e.g., climate, vegetation state (FPAR), and atmospheric transport) vary, showed that the observed seasonal amplitude and trend in atmospheric CO_2 are well reproduced with our CASA_TOMCAT framework, albeit with a bias in the trend in recent years (Figure S8). In terms of SZC, while the modeled trend and magnitude show some bias (Figure S9a), its interannual variability is reproduced with fairly high accuracy ($r = 0.74$, $P<0.1\%$) (Figure S9b). The trend biases in recent years suggest limitations in our model framework, however, the interannual variability of simulated SZC is well reproduced, which is the focus of this work. Thus we can further investigate within our model framework what could cause a breakdown using factorial simulations where the respective model driver of interest was held constant.

The influence of each model driver was assessed by comparing the SZC obtained from that respective factorial simulation (SZC from the SLR simulation is denoted SZC_{SLR}) with the SZC from the CTR simulation (SZC_{CTR}). The SZC obtained from factorial simulations with constant climate drivers (SZC_{TMP}, SZC_{TMO}, and SZC_{SLR}) show nearly perfect correlations with SZC_{CTR}, whereas keeping FPAR constant (SZC_{FPAR}) leads to a significant reduction in correlation with SZC_{CTR}, particularly in the later period (Table 1). SZC_{ALL} (climate and FPAR held constant) has very similar correlations with SZC_{CTR} as SZC_{FPAR}. These results show that NPP through FPAR is the most dominant CASA factor in controlling SZC variability, with an increase in influence in the later period.

In the case of constant transport simulations (denoted by prefix "$AT,$") the correlations with SZC_{CTR} underwent a greater reduction during both periods than SZC_{FPAR} (Table 1). This shows that atmospheric transport had the largest influence on SZC variability throughout the study period, with an increase in dominance in the later period. Simulations that combine interannually nonvarying transport with constant climate

(SZC$_{AT,TMP}$, SZC$_{AT,TMO}$, and SZC$_{AT,SLR}$) show no significant deviation from SZC$_{AT,CTR}$ regarding correlations with SZC$_{CTR}$. SZC$_{AT,FPAR}$ and SZC$_{AT,ALL}$ demonstrate near full absence of the correlation with SZC$_{CTR}$, further indicating that NPP (through FPAR) and atmospheric transport are the two most important factors controlling interannual variability in SZC at Barrow (Table 1).

In regard to correlations between simulated SZC at Barrow and footprint-weighted spring temperature, we first confirm that simulated SZC shows a breakdown with temperature similar to the observed breakdown (Table 1). We then determine the influence of each variable in CASA, as well as atmospheric transport in TOMCAT, on the SZC temperature sensitivity by holding the respective variables constant (while maintaining seasonal variations). If those simulations still show the breakdown, then we can conclude that this variable did not cause the breakdown between the two periods. According to this logic, we find for all CASA variables tested that the breakdown is still strong. We do not find a breakdown when only atmospheric transport is held constant (AT,CTRL). As we only observe a breakdown from the first to the second period with varying transport simulations, but no breakdown when transport is held constant, we can conclude that temperature sensitivity has remained constant throughout the study period, and that atmospheric transport is a driving force behind the breakdown in temperature sensitivity of SZC.

The correlations between simulated SZC and temperature averaged over 50°N differ to a large extent from correlations between footprint-weighted temperature and simulated SZC (Table 1) which further indicates the importance of accounting for interannually varying footprints.

Our model reproduced interannual variations in SCC slightly better than SZC (Figure S23), although there was a similar bias in the trend and magnitude (Figure S24). Analysis of SCC from our factorial simulations yielded similar results to those obtained from SZC analysis, albeit with even greater dominance of atmospheric transport over temperature sensitivity, revealed by consistent correlation between SCC$_{ATCTR}$ and footprint-weighted spring temperature ($r = 0.68$, $P < 0.01$) during both periods (Table S1).

Based on their process-based factorial simulation results, P2017 concluded that transport played no significant role in interannual correlations between SZC and temperature, and that net ecosystem productivity in boreal regions is the dominating factor. Our analysis differs from that of P2017 in that we also compare simulated SZC with the control run (in which all variables vary), as well as simulated SZC with footprint-averaged temperature. We found that atmospheric transport controls a significant proportion of SZC variability, particularly in the later period, which is consistent with our finding that the spatial coherence of temperature anomalies decreased significantly in the late period (Figure S5). Furthermore, when holding atmospheric transport constant (ATCTR), there was no breakdown in temperature sensitivity of SZC (Table 1), whereas when holding NEE constant (ALL), we did witness a breakdown. This illustrates that, contrary to the conclusions of P2017, atmospheric transport is the key driver behind the breakdown in temperature sensitivity of spring carbon uptake. We also compared the simulated SZC with 50°N averaged temperature and found differing results, which highlights the sensitivity of temperature to the footprint. Therefore, this suggests 50°N is not an accurate representation of the air masses seen by Point Barrow, as used by P2017.

4. Conclusions

We are witnessing a phase of changing CO_2 levels and climate to which land vegetation is exposed and is adapting. Over the past decades, atmospheric records and fossil fuel emission inventories indicate that the land carbon sink has been growing, taking up approximately 25% of CO_2 entering the atmosphere as a result of fossil fuel burning and land-use change (Friedlingstein et al., 2019). Other indicators of changes in terrestrial carbon cycling include (amongst others) increasing trends in the seasonal amplitude of atmospheric CO_2 exchanges in the northern high latitudes (Graven et al., 2013). In this regard, a weakening relationship between atmospheric CO_2 drawdown measured at Barrow and above 50°N land surface temperature during Boreal spring have been interpreted as a shift from spring temperature as the main control over plant productivity and consequently spring carbon uptake toward other controls, such as light limitation (P2017). This conclusion is based on the breakdown of the correlation between SZC anomalies and spring temperature anomalies averaged over vegetated land north of 50°N after 1995. Somewhat surprisingly, however, our analysis of NDVI (a proxy for plant productivity) does not indicate a similar breakdown of spring

temperature controls on NDVI after 1995. We, therefore, have attempted to understand why these analyses come to different conclusions.

One aspect which has not been studied in great detail so far is the role of site-specific regions of influence of atmospheric signals, as well as the interplay between the interannual variation of site-specific regions of influence and homogeneity of temperature anomalies. We find that regions of influence are quite localized and vary substantially at an interannual timescale. For the Barrow site, the influence of fluxes from Eurasia versus North America varies interannually, contributing between 30% and 65% of the total land signal (Figure S3). Simulations of the CO_2 signals at high-latitude sites for interannually varying land-atmosphere carbon exchange flux simulated with a data-driven model reveal that anomalies of CO_2 drawdown signals can be very well reproduced when using site-specific regions of influence but not when using above 50°N average surface temperature anomalies. This suggests a major role played by varying atmospheric transport when attempting to properly represent the influence of temperature on SZC anomalies. Furthermore, our factorial simulations reveal that atmospheric transport is strongly influential over SZC variability, particularly in the later period, playing a dominant role in the breakdown of the correlations between SZC and temperature. Thus, the breakdown in correlation between SZC and temperature is not indicative of a breakdown in the temperature sensitivity of spring carbon uptake, and thus is in agreement with the consistent correlation between NDVI and temperature anomalies (Figure 1c).

We furthermore investigated the extent to which the homogeneity of temperature anomalies has changed over the study period. We find a significant shift toward greater spatial heterogeneity in anomalies (Figure S5), likely driven by a sustained, strong Arctic Oscillation during the 1979–1995 period becoming comparatively inactive in the 1996–2012 period (Figure S1). The trend toward greater heterogeneity in the spring temperature anomalies across the northern latitudes in the later period (Figure S5) may explain the increased role of transport in the later period (Figure 1) and may also provide an alternative explanation for the breakdown in the correlations between SZC at Barrow and average northern high latitude spring temperatures as noted by P2017.

Together, these findings suggest that the temperature sensitivity of vegetation during springtime has not changed as significantly across the high latitudes as previously suggested (P2017) and that the increased importance of atmospheric transport due to a change in spatial coherence of the temperature signal is the main factor responsible for the breakdown in correlation between SZC and spring temperature. We found that after accounting for atmospheric transport, the weakening of the temperature sensitivity of spring carbon uptake in the high northern latitudes is substantially smaller than previously asserted. Based on the atmospheric CO_2 data and satellite vegetation data we thus conclude that temperature remains an important control of spring plant carbon uptake above 50°N. Improved understanding of the controls of carbon uptake and release of boreal and arctic ecosystems, primarily forests, helps to forecast how these ecosystems may evolve over coming decades.

Data Availability Statement

Data for this research is available at: https://doi.org/10.5281/zenodo.4297461.

References

Andres, R. J., Boden, T. A., & Marland, G. (2016). *Annual fossil-fuel CO2 emissions: MA of emissions gridded by one degree latitude by one degree longitude*. Tenn., Carbon Dioxide Information Analysis Center, Oak Ridge National Laboratory, U.S. Department of Energy. https://doi.org/10.3334/CDIAC/ffe.ndp058.2016

Buermann, W., Lintner, B. R., Koven, C. D., Angert, A., Pinzon, J. E., Tucker, C. J., & Fung, I. Y. (2007). The changing carbon cycle at Mauna Loa Observatory. *Proceedings of the National Academy of Sciences*, *104*(11), 4249–4254. https://doi.org/10.1073/pnas.0611224104

Chipperfield, M. P. (2006). New version of the TOMCAT/SLIMCAT off-line chemical transport model: Intercomparison of stratospheric tracer experiments. *Quarterly Journal of the Royal Meteorological Society*, *132*(617), 1179–1203. https://doi.org/10.1256/qj.05.51

Ciais, P., Tan, J., Wang, X., Roedenbeck, C., Chevallier, F., Piao, S.-L., et al. (2019). Five decades of northern land carbon uptake revealed by the interhemispheric CO2 gradient. *Nature*, *568*(7751), 221–225. https://doi.org/10.1038/s41586-019-1078-6

Claret, M., Sonnerup, R., & Quay, P. (2021). Next generation global ice-ocean-biogeochemistry coupled model with 13C-cycling (GFDL-MOM5-BLING13C) [Data set]. *Zenodo*. https://doi.org/10.1029/2020gb006757

Dee, D. P., Uppala, S. M., Simmons, A. J., Berrisford, P., Poli, P., Kobayashi, S., et al. (2011). The ERA-Interim reanalysis: Configuration and performance of the data assimilation system. *Quarterly Journal of the Royal Meteorological Society*, *137*(656), 553–597. https://doi.org/10.1002/qj.828

Friedlingstein, P., Jones, M., O'Sullivan, M., Andrew, R., Hauck, J., Peters, G., et al. (2019). Global carbon budget. *Earth System Science Data*, *11*(4), 1783–1838. https://doi.org/10.5194/essd-11-1783-2019

Graven, H. D., Keeling, R. F., Piper, S. C., Patra, P. K., Stephens, B. B., Wofsy, S. C., et al. (2013). Enhanced seasonal exchange of CO_2 by northern ecosystems since 1960. *Science*, *341*(6150), 1085–1089. https://doi.org/10.1126/science.1239207

Harris, I., Jones, P. D., Osborn, T. J., & Lister, D. H. (2014). Updated high-resolution grids of monthly climatic observations - The CRU TS3.10 Data set. *International Journal of Climatology*, *34*(3), 623–642. https://doi.org/10.1002/joc.3711

Keeling, C. D., Chin, J. F. S., & Whorf, T. P. (1996). Increased activity of northern vegetation inferred from atmospheric CO2 measurements. *Nature*, *382*(6587), 146–149. https://doi.org/10.1038/382146a0

McGuire, A. D., Anderson, L. G., Christensen, T. R., Dallimore, S., Guo, L., Hayes, D. J., et al. (2009). Sensitivity of the carbon cycle in the Arctic to climate change. *Ecological Monographs*, *79*(4), 523–555. https://doi.org/10.1890/08-2025.1

Park, H., Jeong, S.-J., Ho, C.-H., Kim, J., Brown, M. E., & Schaepman, M. E. (2015). Nonlinear response of vegetation green-up to local temperature variations in temperate and boreal forests in the Northern Hemisphere. *Remote Sensing of Environment*, *165*, 100–108. https://doi.org/10.1016/j.rse.2015.04.030

Piao, S., Ciais, P., Friedlingstein, P., Peylin, P., Reichstein, M., Luyssaert, S., et al. (2008). Net carbon dioxide losses of northern ecosystems in response to autumn warming. *Nature*, *451*(7174), 49–52. https://doi.org/10.1038/nature06444

Piao, S., Liu, Z., Wang, T., Peng, S., Ciais, P., Huang, M., et al. (2017). Weakening temperature control on the interannual variations of spring carbon uptake across northern lands. *Nature Climate Change*, *7*(5), 359–363. https://doi.org/10.1038/nclimate3277

Pinzon, J., & Tucker, C. (2014). A Non-Stationary 1981-2012 AVHRR NDVI3g Time Series. *Remote Sensing*, *6*(8), 6929–6960. https://doi.org/10.3390/rs6086929

Potter, C. S., Randerson, J. T., Field, C. B., Matson, P. A., Vitousek, P. M., Mooney, H. A., & Klooster, S. A. (1993). Terrestrial ecosystem production: A process model based on global satellite and surface data. *Global Biogeochemical Cycles*, *7*(4), 811–841. https://doi.org/10.1029/93gb02725

Randerson, J. T., Field, C. B., Fung, I. Y., & Tans, P. P. (1999). Increases in early season ecosystem uptake explain recent changes in the seasonal cycle of atmospheric CO_2 at high northern latitudes. *Geophysical Research Letters*, *26*(17), 2765–2768. https://doi.org/10.1029/1999gl900500

Randerson, J. T., Thompson, M. V., Malmstrom, C. M., Field, C. B., & Fung, I. Y. (1996). Substrate limitations for heterotrophs: Implications for models that estimate the seasonal cycle of atmospheric CO_2. *Global Biogeochemical Cycles*, *10*(4), 585–602. https://doi.org/10.1029/96gb01981

Stein, A. F., Draxler, R. R., Rolph, G. D., Stunder, B. J. B., Cohen, M. D., & Ngan, F. (2015). NOAA's HYSPLIT atmospheric transport and dispersion modeling system. *Bulletin of the American Meteorological Society*, *96*(12), 2059–2077. https://doi.org/10.1175/BAMS-D-14-00110.1

Thompson, D., & Wallace, J. (1998). The Arctic oscillation signature in the wintertime geopotential height and temperature fields. *Geophysical Research Letters*, *25*(9), 1297–1300. https://doi.org/10.1029/98GL00950

Thoning, K., Crotwell, & Mund, J. (2020). *Atmospheric carbon dioxide dry air mole fractions from continuous measurements at mauna loa, Hawaii, Barrow, AK, American Samoa and south Pole. 1973-2019, version 2020-08 national Oceanic and atmospheric administration (NOAA)*. Global Monitoring Laboratory (GML). https://doi.org/10.15138/yafl-bk21

Thoning, K. W., Tans, P. P., & Komhyr, W. D. (1989). Atmospheric carbon dioxide at Mauna Loa Observatory: 2. Analysis of the NOAA GMCC data, 1974-1985. *Journal of Geophysical Research*, *94*(D6), 8549–8565. https://doi.org/10.1029/jd094id06p08549

Walther, S., Voigt, M., Thum, T., Gonsamo, A., Zhang, Y., Köhler, P., et al. (2016). Satellite chlorophyll fluorescence measurements reveal large? Scale decoupling of photosynthesis and greenness dynamics in boreal evergreen forests. *Global Change Biology*, *22*(9), 2979–2996. https://doi.org/10.1111/gcb.13200

Wang, K., Wang, Y., Wang, X., He, Y., Li, X., Keeling, R. F., et al. (2020). Causes of slowing-down seasonal CO 2 amplitude at Mauna Loa. *Global Change Biology*, *26*(8), 4462–4477. https://doi.org/10.1111/gcb.15162

Wang, Y., Li, M., & Shen, L. (2013). Accelerating carbon uptake in the Northern Hemisphere: Evidence from the interhemispheric difference of atmospheric CO2 concentrations. *Tellus B: Chemical and Physical Meteorology*, *65*(1), 20334. https://doi.org/10.3402/tellusb.v65i0.20334

Zhu, Z., Bi, J., Pan, Y., Ganguly, S., Anav, A., Xu, L., et al. (2013). Global Data Sets of Vegetation Leaf Area Index (LAI)3g and Fraction of Photosynthetically Active Radiation (FPAR)3g Derived from Global Inventory Modeling and Mapping Studies (GIMMS) Normalized Difference Vegetation Index (NDVI3g) for the Period 1981 to 2011. *Remote Sensing*, *5*, 927–948. https://doi.org/10.3390/rs5020927